Magnetic Polystyrene Nanocomposites Reinforced with Magnetite Nanoparticles

Xingru Yan, Qingliang He, Xi Zhang, Hongbo Gu, Haoran Chen, Qiang Wang, Luyi Sun, Suying Wei,* Zhanhu Guo

Polystyrene (PS)/magnetite (Fe_3O_4) polymer nanocomposites (PNCs) are successfully synthesized by a solvent extraction method. Scanning electron microscopy reveals that the nanoparticles are well distributed in the PS matrix with 5, 10, and 20 wt% without obvious agglomeration. Fourier transform infrared spectroscopy analysis indicated that the PS/Fe_3O_4 PNCs are synthesized with strong interaction between PS and nanoparticles. The thermogravimetic analyzer and microscale combustion calorimetry reveal an enhanced thermal stability and reduced flammability. The differential scanning calorimetry demonstrates both glass transition temperature (T_g) and melting temperature (T_m) increased with increasing the Fe_3O_4 nanoparticle loading. The observed monotonically decreased complex viscosity indicates a strong shear thinning behavior in the PNCs; meanwhile, the percolation takes place in the low frequency range (0.1–1 Hz) when the nanoparticles are introduced in the matrix. The T_g of the PS/Fe_3O_4 nanocomposites determined from the dynamic mechanical analysis shifts to a higher temperature compared with that of pure PS. Enhanced dielectric properties relate to the Fe_3O_4 NP loadings. In addition, the PS/Fe_3O_4 PNCs exhibit superparamagnetic behavior at room temperature.

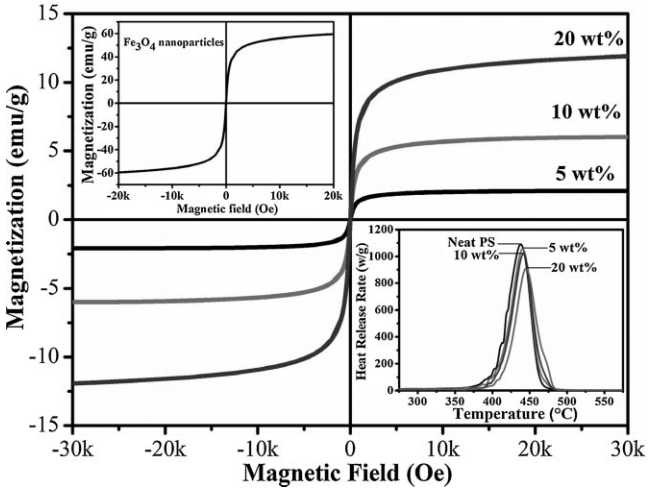

S. Wei, X. Yan, X. Zhang, H. Gu
Department of Chemistry and Biochemistry, Lamar University, Beaumont, TX 77710, USA
E-mail: suying.wei@lamar.edu
Z. Guo, X. Yan, Q. He, X. Zhang, H. Gu
Integrated Composites Laboratory (ICL), Dan F. Smith Department of Chemical Engineering, Lamar University, Beaumont, TX 77710, USA
E-mail: zhanhu.guo@lamar.edu
H. Chen, L. Sun
Department of Chemistry and Biochemistry, Texas State University, San Marcos, TX 78666, USA
Q. Wang
College of Environmental Science and Engineering, Beijing Forestry University, Beijing 100083, China

1. Introduction

Magnetic polymer nanocomposites (PNCs) have captured intense attention owing to their unique physicochemical properties and manifold potential applications including energy storage devices,[1] magnetic sensors,[2] fire retardants,[3] microwave absorbers,[4,5] and magnetic recording information.[6] Magnetic properties can be obtained by either physical or chemical methods, such as surface initiated polymerization,[7] in situ polymerization,[8] solution blending,[9,10] melt blending,[11] layer-by-layer deposition,[12] and surface wetting method,[13] to incorporate magnetic nanoparticles (NPs) including iron,[14] cobalt,[15] nickel,[16] and their alloys in the non-magnetic polymer

DOI: 10.1002/mame.201300208

matrix. Magnetic NPs cannot only introduce the magnetization but also improve the thermal stability,[17] mechanical property,[18] optical property,[19] combustion properties,[3] and dielectric property[20] through combining the merits of the organic polymer matrix and the inorganic components with different nanostructures and sizes. Compared with other magnetic NPs, magnetite NPs (Fe_3O_4) are considered as one of the most promising materials due to the fairly large magnetization and admirable conductive properties.[21]

Polystyrene (PS) is one of the most important polymers of today. Its popularity stems from the fact that it possesses many unique properties, such as good processability, rigidity, transparency, low water absorbability, and that it can be produced at low cost. Therefore, there are several studies in literature about PS with Fe_3O_4 NPs. Huang and Tang[22] have prepared core–shell structure particles comprising nearly monodisperse PS spheres as cores and Fe_3O_4 as shells. By using slow injection, the thickness of the shell was controlled in the range of 0–60 nm. After studying the composite and the structure of the shell, it is found that there are some differences between the magnetic composite spheres shelled with Fe_3O_4 and pure Fe_3O_4 particles, such as the size of the magnetite and the ferromagnetic property. Meanwhile, the spheres exhibited the superparamagnetic characteristic when the thickness of the Fe_3O_4 shell was $<$15 nm. Zhao and Yi[23] have prepared PS/Fe_3O_4 composite microspheres by an emulsion polymerization method. The modified Fe_3O_4 NPs were copolymerized with styrene and acrylic acid to form the magnetic polymer microspheres with carboxyl groups to study the preparation of the nanosized, monodisperse, cross-linked, magnetic composite polymer microspheres. Zhong et al.[24] have investigated the PS/Fe_3O_4 composites synthesized by a facile in situ bulk radical polymerization. Shi et al.[25] reported polyethylene-oxide-modified PS/Fe_3O_4 nanospheres synthesized by the miniemulsion/emulsion polymerization with quantum dots (QDs) as a second nanofiller. The QDs immobilized on the surfaces of magnetic Fe_3O_4 composite nanospheres exhibit intense visible-light emission in the fluorescence spectroscopy. Meanwhile, the Fe_3O_4 NPs respond to an external magnetic field by increasing the temperature of the surrounding environment, which can be used therapeutically. Although the morphology, superparamagnetic properties and thermal stability of the fabricated PS/Fe_3O_4 PNCs have been reported, the dielectric permittivity, melt rheological behavior, flammability, and thermo-mechanical properties of the PS/Fe_3O_4 PNCs fabricated using solvent extraction method have not been reported.

In this work, the PS/Fe_3O_4 nanocomposites with various Fe_3O_4 particle loadings were prepared by a facile solvent extraction method. The scanning electron microscope (SEM) was used to characterize the dispersion quality of Fe_3O_4 NPs and the morphology of the PS/Fe_3O_4 nanocomposites. The effects of the Fe_3O_4 NPs on the crystallization behaviors of PS were also studied by X-ray diffraction (XRD) and differential scanning calorimetry (DSC). The chemical structures of the PS/Fe_3O_4 nanocomposites were characterized by Fourier transform infrared (FT-IR) spectroscopy. The thermal stability of the PS/Fe_3O_4 nanocomposites was tested by thermogravimetric analysis (TGA). The effects of the particle loading on the storage/loss modulus of the PS/Fe_3O_4 nanocomposites were studied systematically. The thermo-mechanical, magnetic, dielectric, and flammability properties were also studied and discussed.

2. Experimental Section

2.1. Materials

Polystyrene (melt flow rate = 9.0, $\overline{M}_n$ = 83 900, $\overline{M}_w$ = 2 25 600) was supplied by Total Petrochemicals USA, Inc. Anhydrous *N,N*-dimethylformamide (DMF, 99.9%) was purchased from Alfa Aesar. The Fe_3O_4 NPs were provided by Nanjing Emperor Nano Material Co., Ltd., China. All the materials were used as received without any further treatment.

2.2. Preparation of PS/Fe_3O_4 Nanocomposites

The PS/DMF solutions were prepared by magnetic stirring at room temperature with a polymer loading of 30 wt% until PS was completely dissolved. Different loadings of Fe_3O_4 NPs (5, 10, and 20 wt% with regard to the weight of PS and NPs) were then added to the PS/DMF solutions. After completely wetting the NPs with the polymer solution, both mechanical stirring (400 rpm, 90 min) and ultrasonication (90 min) were subsequently performed to disperse the NPs in the PS solution. The NP suspended solutions were then transferred to deionized water to immobilize the Fe_3O_4 NPs in the PS matrix. The PNCs were precipitated immediately from the DI water by using a solvent extraction process. After that the PNCs were dried in a vacuum oven at 60 °C for 48 h to eliminate the residue DMF and DI water. Pure PS was also prepared from the same procedures without adding the Fe_3O_4 NPs.

2.3. Characterization

The morphologies of pure PS and its Fe_3O_4 nanocomposites were characterized using a Helios NanoLab 400 DualBeam SEM. The SEM specimens were coated with a thin gold for better imaging. The crystalline structure of pure PS and its PNCs was studied by XRD, which was carried out by a Bruker AXS D8 Discover diffractometer operating with a Cu K_α radiation source. The X-ray was generated at 40 kV and 27 mA power and XRD scans were recorded at 2θ from 5 to 80° (λ = 0.154 nm). The FT-IR spectra of the products were carried out by using a Bruker Tensor 27 FT-IR spectrometer with Hyperion 1000 attenuated total reflection (ATR) microscopy accessory in the range 500–4 000 cm^{-1} at a resolution of 4 cm^{-1}.

The thermal stability of pure PS and its Fe_3O_4 nanocomposites was investigated by TGA (TA-Q500 instrument). The heating rate

was 10 °C · min^{-1}, and the experiments were performed in a continuous air flow at a flow rate of 20 mL · min^{-1}. The temperature was ranged from 25 to 700 °C. The effects of the NPs on the thermal properties of PS were determined by using DSC (TA-Q2000 instrument). Heating scans were performed at a rate of 10 °C · min^{-1} in a continuous nitrogen flow rate of 50 mL · min^{-1}. Samples were sealed in a standard aluminum pan and the measurements were taken between 25 and 250 °C. The weight of each sample was approximately 10 mg. The DSC heat flow and temperature values were calibrated with an indium standard.

A Govmark MCC-2 microscale combustion calorimetry (MCC) was utilized to test the flammability of PS nanocomposites according to ASTM D7309-2007 (Method A). In a typical measurement, about 3 mg of the sample was heated from 80 to 650 °C using a linear heating rate of 1 °C · s^{-1} in a stream of nitrogen flow rate of 80 mL · min^{-1}. The thermal degradation products of the sample in nitrogen were mixed with a 20 mL · min^{-1} stream of oxygen prior to entering the 900 °C combustion furnace to complete the non-flaming combustion. The rate and amount of heat were measured by MCC using oxygen consumption calorimeter, which was produced by a complete combustion of fuel gases generated during the controlled pyrolysis of a milligram size specimen.

Dynamic mechanical analyses (DMA) were studied by the TA Instruments AR 2000ex instrument in the torsion rectangular mode with a strain of 0.4% and a frequency of 1 Hz. The temperature range was from 30 to 140 °C. The melt rheological behaviors of neat PS and its PNCs were investigated by TA Instruments AR 2000ex Rheometer. The frequency sweep was from 100 to 0.1 Hz. An environmental test chamber (ETC) steel parallel-plate geometry was used to perform the measurements at 230 °C in the linear viscioelastic (LVE) range with 1% strain under air atmosphere.

The magnetic properties were carried out in a 9 T Physical Properties Measurement System (PPMS) by Quantum Design at room temperature. Agilent E4980A Precision LCR Meter (20 Hz to 2 MHz) with a signal voltage range of 0–2.0 V_{rms} and signal current range of 0–20.0 mA_{rms} was used to collect the dielectric data at room temperature. The samples used were 25 mm in diameter with ca. 2 mm thickness prepared from hot press machine at 190 °C. The frequency was ranged from 500 Hz to 2 MHz.

3. Results and Discussion

3.1. Morphology

The nanofiller size and the morphology play a very important role in determining the performance of the PNCs. Meanwhile, the properties of PNCs depend on the level of dispersion quality of the nanofillers. The morphological characterization is the most direct way to evaluate the level of the nanofiller dispersion. Figure 1 shows the SEM images of the cross-sectional surface of (a) pure PS and the PNCs with a particle loading of (b) 5, (c) 10, and (d) 20 wt%, respectively. The NPs were observed to be well dispersed in the PS matrix with 5, 10, and 20 wt% without obvious agglomeration of Fe_3O_4 NPs.

3.2. X-Ray Diffraction

Figure 2 shows the XRD patterns of the neat PS and PS/Fe_3O_4 PNCs with different weight percentages. The diffraction peaks at $2\theta = 30.2$, 35.6, and 57.2°, correspond to (*220*), (*311*), and (*511*) crystallographic planes of the crystalline Fe_3O_4 content.[26,27] According to the Scherrer Equation (1), the average crystallite size can be estimated by XRD pattern,[28]

$$L = \frac{k\lambda}{\beta\cos\theta} \quad (1)$$

where L is the average crystallite size, k the shape factor, λ the wavelength ($\lambda = 0.154$ nm), β the full width at half maximum, and θ is the angle at maximum intensity. The value of k depends on several factors, including the Miller index of the reflection plane and the shape of the crystal, which is normally 0.89 if the shape is unknown. Here, the peak of the PS/Fe_3O_4 NPs with a particle loading of 10 wt% at

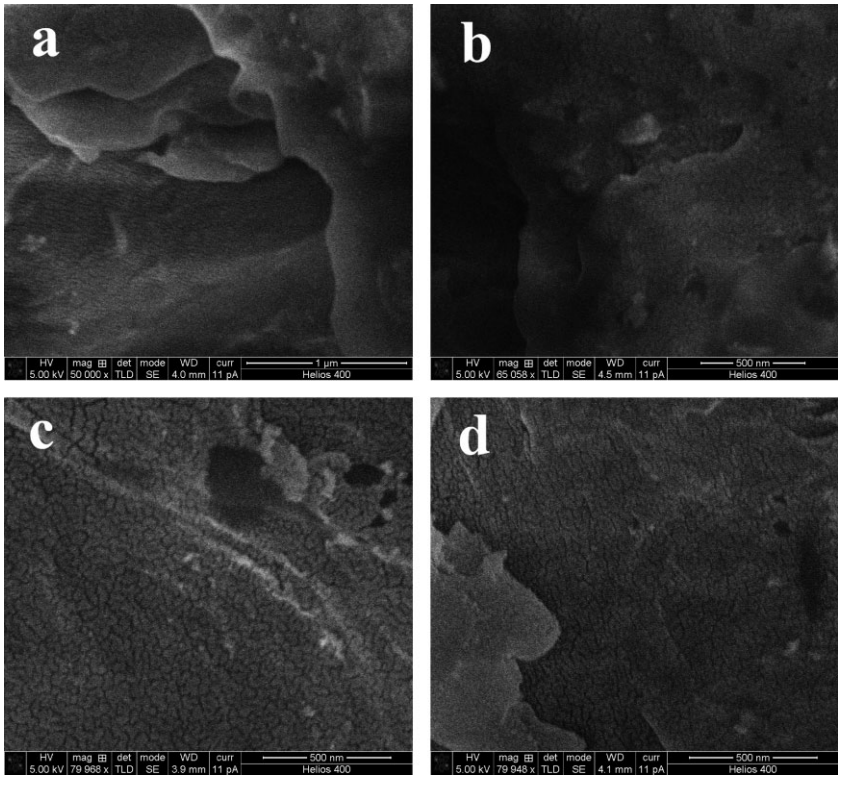

Figure 1. SEM images of the (a) pure PS and the PNCs with a particle loading of (b) 5 wt%, (c) 10 wt%, and (d) 20 wt%, respectively.

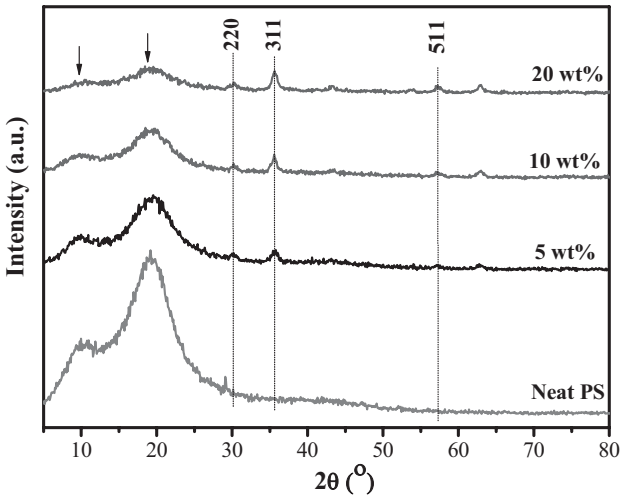

Figure 2. XRD patterns of pure PS and PS/Fe_3O_4 nanocomposites.

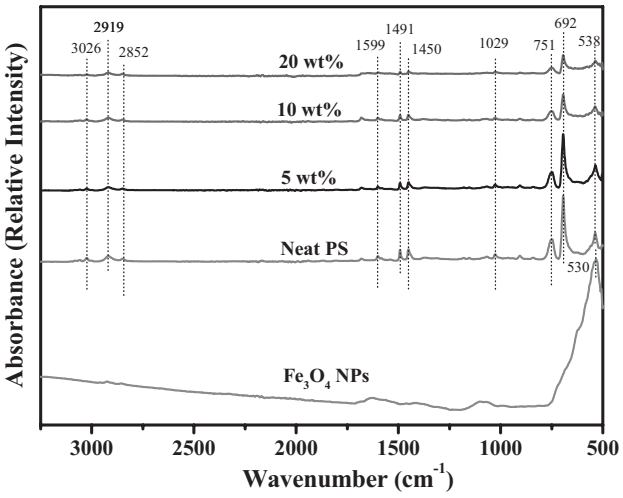

Figure 3. FT-IR spectra of pure PS and its PS/Fe_3O_4 nanocomposites.

$2\theta = 35.6^\circ$ was chosen to calculate the crystallite size, and the average crystallite size of the Fe_3O_4 NPs is about 13.59 nm. The intensity of these diffraction peaks of the Fe_3O_4 NPs becomes stronger with increasing the NP loadings. A hump at 9.8° and a wide peak at 19° are characteristic of crystalline PS, Figure 2, which shows a reduced intensity.[29,30] This indicates a strong interaction between PS backbone and Fe_3O_4 NPs as confirmed by the following FT-IR spectrum analysis. According to all the results, Fe_3O_4 NPs have an affirmative influence on the crystallite of PS.

3.3. FT-IR Spectra

Figure 3 shows the FT-IR spectra of the as-received Fe_3O_4 NPs, pure PS and its nanocomposites reinforced with different NP loadings. The peaks at 692, 751, 1 029, 1 450, 1 491, 1 599, 2 852, 2 919, and 3 026 cm^{-1} are characteristic of styrene absorption.[31] The absorption peak at around 530 cm^{-1} is attributed to the vibration of Fe–O band in the Fe_3O_4 NPs, and shifts from 530 cm^{-1} (in the pure Fe_3O_4 NPs)[32] to 538 cm^{-1} (in the PS/Fe_3O_4 PNCs), which indicates that the PS/Fe_3O_4 nanocomposites have been successfully synthesized with certain interaction between PS and NPs.

3.4. TGA

Figure 4A shows the TGA weight loss curves of neat PS and PS/Fe_3O_4 PNCs, and Figure 4B shows the corresponding derivative weight loss curves. The normalized sample mass is slightly less than 100% after 260 °C, which is attributed to the elimination of moisture in the samples. The major weight loss of all the samples from 260 to 430 °C is due to a large scale thermal degradation of the PS chains.[26,27,33]

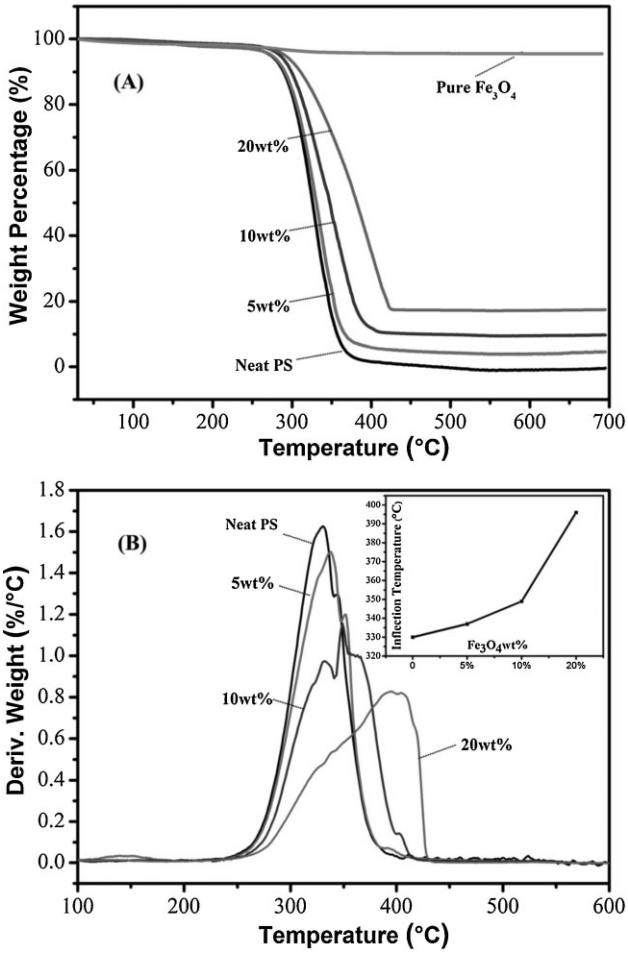

Figure 4. A) TGA weight loss curves and B) derivative weight loss curves of pure PS, Fe_3O_4 and PS/Fe_3O_4 PNCs. Inserted: the inflection point as a function of the loading of Fe_3O_4 NPs.

The Fe_3O_4 sample is also slightly less than 100% due to the loss of moisture and impurities. The weight residues of the PNCs with an initial NP loading of 5.0, 10.0, and 20.0 wt% are 4.5, 9.8, and 17.5%, respectively. The loading noticeably increased, and the corresponding temperature of the maximum rate of the weight loss increased as well, which are shown by the insert in Figure 4B. As the Fe_3O_4 loading increases, the decomposition temperature is correspondingly increased in the PS/Fe_3O_4 PNCs.

The onset degradation temperatures (T_{on}), the 10% mass loss temperature ($T_{10\%}$) and the temperatures of the maximum weight loss rate (inflection point, T_{max}) are summarized in Table 1. The results indicate that the Fe_3O_4 NP loading is not proportional to the onset degradation temperature. For example, the degradation temperature of the PNCs with a 10 wt% Fe_3O_4 NP loading is 12 °C higher than that of the PNCs at 5 wt% Fe_3O_4 NP loading and is increased by 6 °C from 10 to 20 wt%, but only 3 °C from pure PS to the PNCs with a 5 wt% particle loading. The temperature of onset degradation (T_{on}), temperature of 10% mass loss ($T_{10\%}$), and the inflection point (T_{max}) are observed to increase with increasing the Fe_3O_4 NPs loading, listed in Table 1, which shows that the presence of Fe_3O_4 NPs stabilizes PS. The enhanced thermal stability in the PNCs has been reported in the other systems as well.[34–37] The enhanced thermal stability of the PS/Fe_3O_4 PNCs results from the interaction between PS matrix and the Fe_3O_4 NPs. The surface of the Fe_3O_4 NPs absorbs the free radicals produced in the decomposition of PS and restricts the mobility of the polymer molecules, which retards the degradation of the PS/Fe_3O_4 PNCs.[38,39]

3.5. DSC Analysis

Figure 5 shows the DSC thermograms of PS nanocomposites with different Fe_3O_4 NP loadings, based on which the effects of the incorporated Fe_3O_4 NPs on the PS matrix can be explored from the aspects of both glass transition temperature (T_g) and melting temperature (T_m). The addition of Fe_3O_4 NPs in the PS matrix is observed to have a marginal effect on the T_g of PS and slightly increase T_m compared to that of neat PS, Figure 5. In addition, Uthirakumar et al.[40] have reported an improved T_g in the PS nanocompsites filled with montmorillonite. Both the confined polymer chains between the layers of fillers and the restricted segmental motions at the organic–inorganic interface are responsible for the increased T_g.[40]

Table 1. TGA data of the pure PS and PS/Fe_3O_4 nanocomposites.

Fe_3O_4 loading [wt%]	Neat PS	5 wt%	10 wt%	20 wt%
T_{on} [°C]	272	275	287	293
$T_{10\%}$ [°C]	289	292	299	311
T_{max} [°C]	330	337	349	396

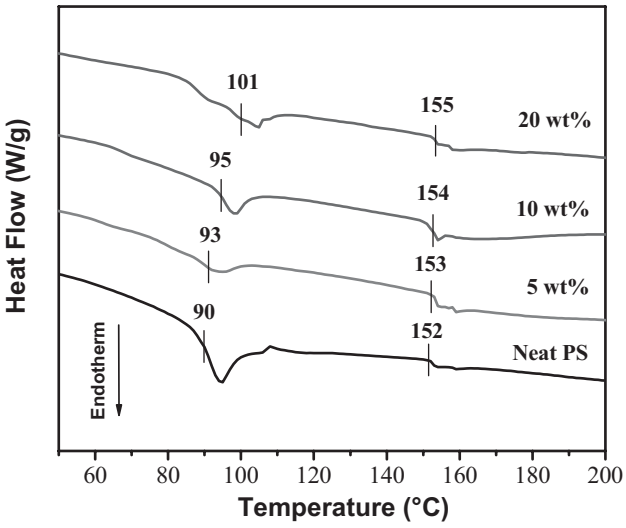

Figure 5. DSC thermograms of pure PS and PS/Fe_3O_4 nanocomposites with different Fe_3O_4 nanoparticle loadings.

With a Fe_3O_4 NP loading of 10 and 20 wt%, the melting temperatures of the PNCs are around 2 and 3 °C higher than that (152 °C) of the pristine PS, respectively. The result of this phenomeon is the retarded mobility of the PS chains surrounded by Fe_3O_4 NPs and a subsequently higher temperature is needed to move the entire long polymer chains.[10] Noticeably, an increase in the Fe_3O_4 loading leads to wider and shallower exothermic curves, which indicate that the dispersed Fe_3O_4 NPs act as barriers to the formation of large PS crystallites.[41]

3.6. Flammability Properties

Microscale combustion calorimetry was further utilized to evaluated the flammability of PS and its PNCs with different particle loadings by studying the heat release rate (HRR) as a function of temperature, Figure 6, and the heat release capacity (HRC), peak heat release rate (PHRR), total heat release (THR), and maximum pyrolysis rate (T_{PHRR}) are summarized in Table 2. HRR is the most important variable to assess the flammability and fire hazard of materials.[42] Meanwhile, a relatively good indicator of the HRR is the HRC in the propensity for ignition and flaming combustion. And a low value of HRC means low full fire hazard and low flammability.[43] PHRR is the maximum HRR when one sample generates the highest rate of heat release. Compared with that of pure PS, the PHRR value of the PNCs with 20 wt% NPs loading is decreased by 16.28%. The HRC of the PS/Fe_3O_4 PNCs has a similar change trend as PHHR, Table 2, which can be attributed to the existence of Fe_3O_4 NPs. In addition, the THR and maximum pyrolysis

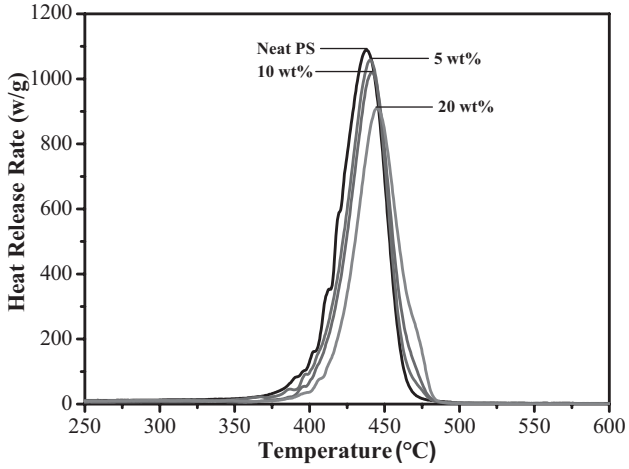

Figure 6. The HRR curves of PS/Fe_3O_4 nanocomposites with a particle loading of 5, 10, and 20 wt%, respectively.

rate (T_{PHRR}) decreases with increasing the particle loading. These are due to a higher initial thermal stability of pure Fe_3O_4 than that of pure PS shown in the TGA results, which can also explain the phenomenon that the temperature corresponding PHRR increases with increasing the Fe_3O_4 NPs loading. Apparently, the Fe_3O_4 NPs as metal component can favor the char formation in the organic materials by reducing the reactive radical during depolymerization process.[44] In addition, the formed char on the surface of materials can prevent the polymeric material from fast decomposition by obstructing heat being transferred from the heat source to the inner material[22] which further suggests that the Fe_3O_4 NPs play a positive role in reduced flammability in PS matrix.

3.7. Thermo-Mechanical Properties

Dynamic mechanical analysiswas used to characterize the viscoelastic properties of the materials by providing specific information on the storage modulus (E'), loss modulus (E''), and tanδ within the investigated temperature range.[45] The E' reflects the elastic modulus of nanocomposites, meanwhile, the E'' is related to the energy dissipation associated with the motion of polymer chains due to the friction.[17,46] (The detailed results of E', E'', and tanδ are shown in Figure S1 in the Supporting Information.) The variation of E' of neat PS and PS/Fe_3O_4 nanocomposites as a function of temperature is presented in Figure 7. Compared to neat PS, E' for the PS/Fe_3O_4 PNCs is observed to slightly increase with increasing Fe_3O_4 NP loading within

Table 2. MCC data of pure PS and PS/Fe_3O_4 nanocomposites.

Samples	HRC [$J \cdot g^{-1} \cdot K^{-1}$]	PHRR [$w \cdot g^{-1}$]	THR [$kJ \cdot g^{-1}$]	T_{PHRR} [°C]
Neat PS	1010	1081	38.4	437.8
5 wt%	988	1049	35.1	440.3
10 wt%	958	1016	34.2	441.7
20 wt%	847	905	31.7	445.1

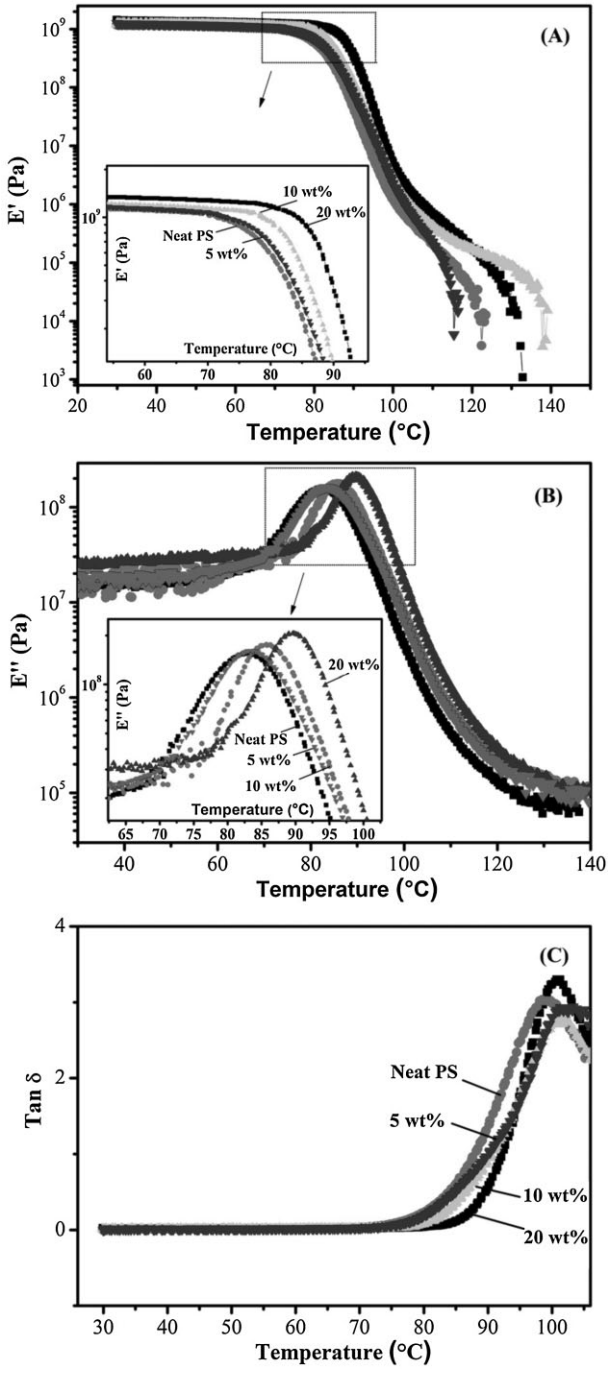

Figure 7. A) Storage modulus (E'), B) loss modulus (E''), and C) tanδ versus temperature for the neat PS and its nanocomposites with different Fe_3O_4 nanoparticle loadings.

the glassy plateau (at 30 °C). This is due to the confinement of the Fe_3O_4 NPs in the matrix. The reason for the slight increase is due to the agglomeration of Fe_3O_4 NPs. Thus, the DMA data agrees well with the rheological properties. A similar trend for E'' is observed as a function of temperature, Figure 7B. The PS PNCs reinforced with 20 wt% Fe_3O_4 NPs within the glassy plateau range exhibit the hightest E'', which is increased from 83 to 90 °C as compared with that of the neat PS. This is attributed to the constrained friction between polymer chains after adding Fe_3O_4 NPs in the PS matrix.[47]

Figure 7C depicts the temperature dependent tanδ of neat PS and its PNCs. The tanδ is the ratio of E'' to E' and the peak of tanδ is often used to determine the glass transition temperature (T_g) of the materials. The T_g of the PNCs increases 2–3 °C compared with neat PS, and this is in agreement with the DSC results discussed in the previous section. This phenomenon is due to the segmental immobilization of matrix chains in the presence of Fe_3O_4 PNs.[48]

3.8. Melt Rheological Behavior

The rheological behaviors of the PNC melts are essential to further investigate the dynamics of the nanoconfined polymer. Also the formation of a percolated system can be detected by characterizing the storage modulus (G'), loss modulus (G''), mechanical loss factor (tanδ), and complex viscosity (η^*) as a function of frequency.[49–51] The PS chains were fully relaxed in the absence of any NPs and revealed a typical homogeneous polymer-like terminal behavior on the basis of melting at 230 °C. G' is observed to increase monotonically with increasing particle loading in all frequency range, Figure 8A. The G' of PNCs with different particle loadings exhibits a larger enhancement at lower frequency than that at higher frequency, due to the presence of the NPs that restrain the large scale polymer chain relaxations in the PNCs if the frequency is low enough.[44] Moreover, a percolation plateau was observed at low frequency range (0.1–1 Hz) when the NPs were introduced in the matrix expect the pure PS sample. However, G' of the PNCs with 20 wt% particle loading is lower than that of the PNCs with 10 wt% particle loading at low frequency, which indicates the dimensions of Fe_3O_4 NPs becomes large leading to the decreased obstruction for polymer chain relaxations. Obviously, the effect of the particle loading on the rheological properties is relatively weak at high frequency, which indicates that the short range dynamics of the PS chains are not significantly

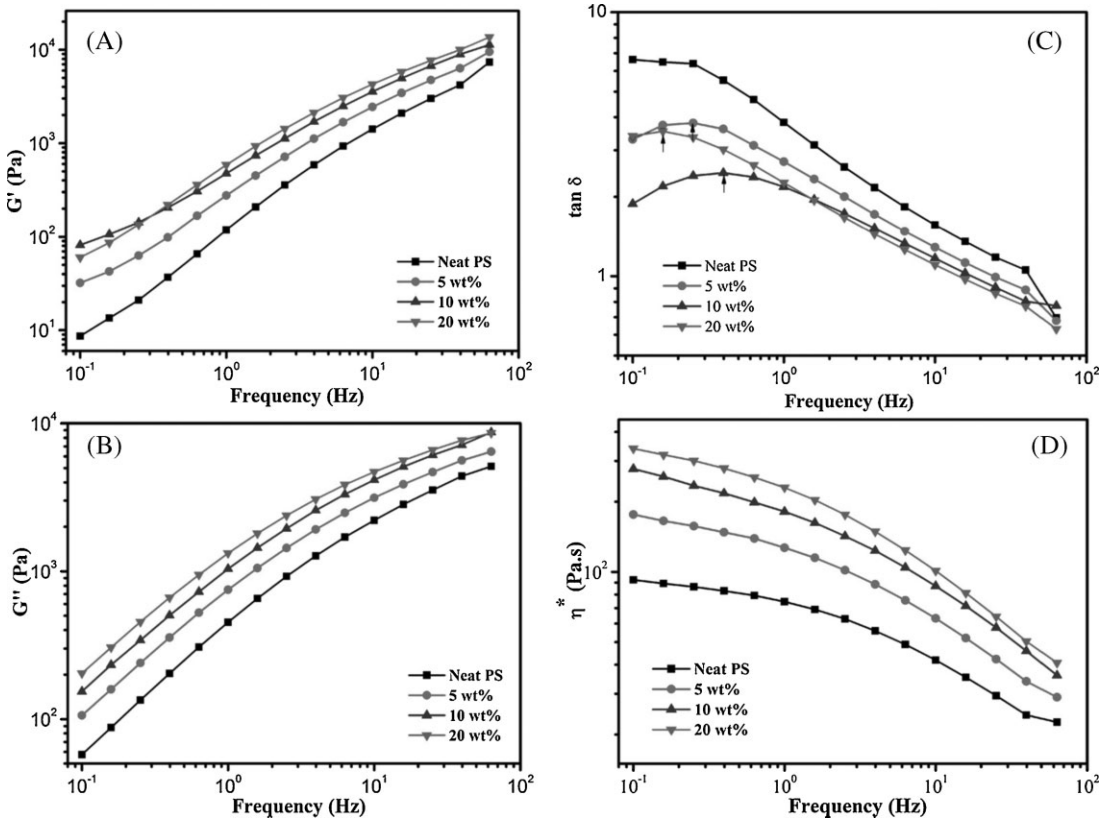

Figure 8. A) Storage modulus (G'), B) loss modulus (G''), C) mechanical loss factor (tanδ), and D) complex viscosity (η^*) as a function of frequency for PS and its PNCs.

affected by the NPs.[20] Similar curve of G'' is observed linearly increased upon incorporation of the NPs in the PS matrix and further increased with increasing the frequency in Figure 8B.

Figure 8C shows the tanδ as a function of frequency. The tanδ is the ratio of G'' to G', which is highly related to the applied frequency. When scanning the experimental frequency from low to high, the tanδ of the PNCs decreases with increasing particle loading. The higher tanδ of neat PS compared to the PNCs is due to the free relaxation of the PS chains. After adding the NPs, the polymer chain relaxation and relative motion have been greatly restrained. Furthermore, the higher the particle loading, the lower the tanδ is. The reason is that the interaction between the NPs and the polymer matrix increases as the particle loading increases, which is in good agreement with the FT-IR results. In addition, a broad peak is observed in all the PNCs except the pure PS sample. The peak position shifts to higher frequency in the PNCs with 5 and 10 wt% particle loadings, which is due to the increased restrictions. However, the peak position of 20 wt% particle loading shifting to a lower frequency is due to the agglomeration of Fe_3O_4 NPs, which hinders the energy dissipation and relaxation between the NPS and polymer matrix.

Figure 8D illustrates the complex viscosity (η^*) of neat PS and its PNCs in a log–log plot of the viscosity as a function of frequency. The η^* is observed to increase with increasing particle loading, especially at low frequencies such as 0.1 Hz. The interaction between Fe_3O_4 and PP matrix restricts the PS chain movements as the Fe_3O_4 particle loading increases. The decreased viscosity with increasing shear rate or frequency is defined as shear thinning.[52] The PNCs with a particle loading of 5 wt% are much more viscous than that of neat PS at low frequency and exhibit strong shear thinning behavior; meanwhile, this property is more evident with increasing the particle loadings. The similar value of η^* at high frequency (10–100 Hz) indicates a polymer melt rather than NPs dominated fluid dynamics.

3.9. Magnetic Properties

Figure 9 shows the room temperature magnetic hysteresis loops of PS nanocomposites with different particle loadings. The insert of Figure 9 shows the as-received pure Fe_3O_4 NPs. The saturation magnetization (M_s) is defined as the state, at which the magnetic field cannot increase the magnetization of the material further.[20] The pure PS is observed to be non-magnetic as expected, whereas the curves of the others show no hysteresis loops. The M_s of the as-received Fe_3O_4 NPs was not reached even at high magnetic field and was determined by the extrapolated saturation magnetization obtained from the intercept of $M \approx H^{-1}$ at high field.[53,54] The PNCs do not

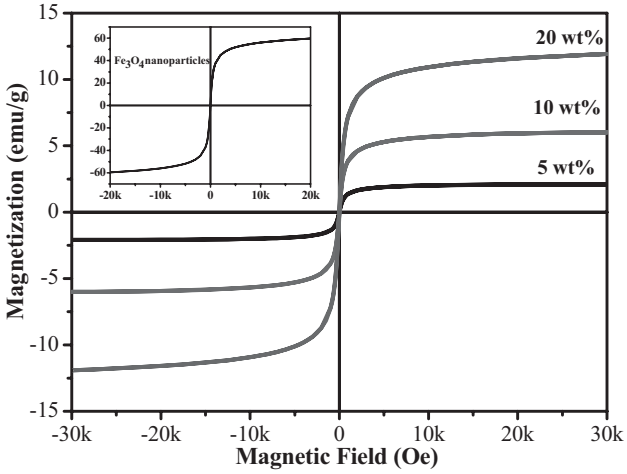

Figure 9. Room temperature hysteresis loops of PS/Fe_3O_4 nanocomposites with a particle loading of 5, 10, and 20 wt%, respectively; insert shows pure NPs.

show hysteresis loop with zero coercivity, which indicates that the superparamagnetic behavior at room temperature.[55] The calculated M_s of the as-received Fe_3O_4 NPs is 57.38 emu $\cdot$ g^{-1}, which is smaller than the bulk Fe_3O_4 (92–100 emu $\cdot$ g^{-1}).[56] The M_s values of the PS/Fe_3O_4 PNCs with particle loadings of 10 and 20 wt% are observed to be saturated at a lower field and are about 6.1 and 11.9 emu $\cdot$ g^{-1}, respectively. In addition, the magnetization saturated more rapidly in the PNCs with a lower NP loading. The particle loadings for 10 and 20 wt% estimated from the M_s are calculated to be 10.6 and 20.7%, which is consistent with the results obtained from TGA. The field required to saturate the magnetization of the 20 wt% sample is exponentially large and beyond the limit of the measurement. An infinitesimal coercivity was observed in all the samples, which indicates a superparamagnetic behavior of the NPs disregard of the presence statues in the polymer matrix.[10]

3.10. Dielectric Properties

Various PS PNCs with Fe_3O_4 NPs have been investigated for their potential applications in energy storage through measuring their dielectric property.[57,58] Dielectric materials can be used to store electrical energy through charge separation, which occurs when the electron distributions are polarized by an applied external electric field.[59] Figure 10A depicts the frequency dependent real permittivity (ε') of these PNCs at 25 °C. The ε' of neat PS is about 3.6. The ε' of the PS PNCs incorporated with 5, 10, and 20 wt% of Fe_3O_4 slightly increased to 4.2–5.0. In addition, for the PNCs with low permittivity, the value of ε' in the PS PNCs is virtually independent of the frequency, indicating a stable dielectric performance of the prepared PNCs

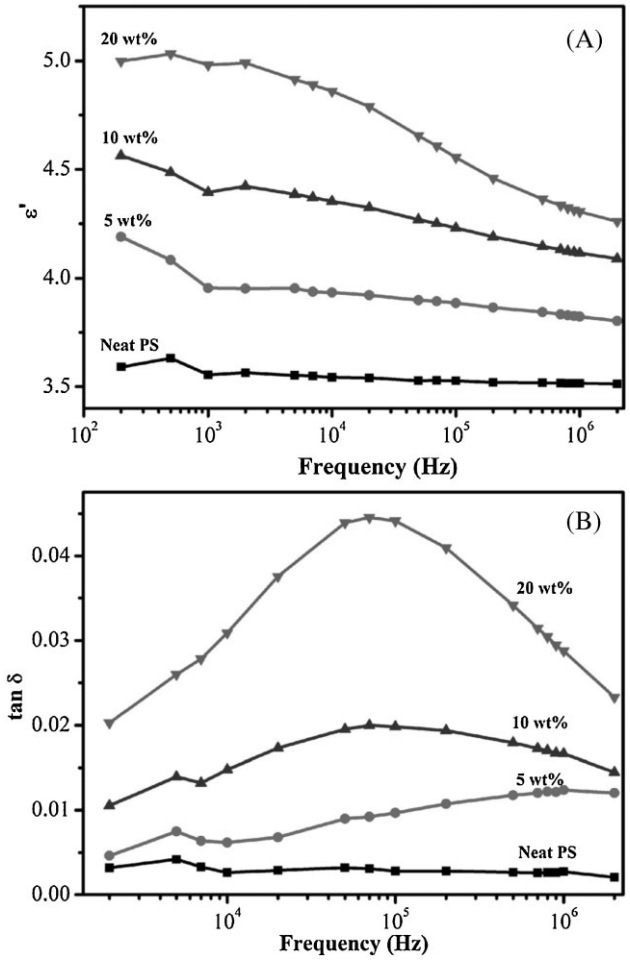

Figure 10. A) Real permittivity, B) dielectric loss tangent as a function of frequency for neat PS and its PNCS with different nanoparticle loadings.

upon frequency variation. Their permittivity gradually decreased with increasing frequency and was stabilized at ca. 3.8, 4.2, and 4.4 for the PNCs with 5, 10, and 20 wt%, respectively, at frequencies higher than 10^6 Hz. The step-like decrease of the ε' toward high frequency is induced by the dielectric relaxation, suggesting that the established percolation network structure is not stable and easily affected by the external frequency disturbances, similar to the poly (vinylidene fluoride)/MWCNTs and elastomer/CNF PNCs.[60,61]

Figure 10B shows the frequency dependent dielectric loss (tanδ). The tanδ value was observed to be slightly enhanced in the PNC with a particle loading of 5 wt% and the tanδ value fluctuated with increasing oscillation frequency. However, the curves of the nanocomposites filled with 10 and 20 wt% Fe_3O_4 NPs reach a peak value at around 10^5 Hz from the low frequency. After that, both curves decrease toward high frequency. The peak in 20 wt% Fe_3O_4 PNC sample is sharper than that of 15 wt% Fe_3O_4 PNCs. These phenomena reveal that the insulating layer is unstable and can be easily affected by the increased frequency. The insulating PS layer, which was wrapped physically on the surface of NPs, became thinner and not sufficient to hold the charge carriers of the Fe_3O_4 NPs.[62] Since large amount of electric energy storage is required in mobile electronic devices, hybrid electric vehicles, stationary power systems, and pulse power applications,[58,63] there is growing attention in the study of the dielectric property of new materials.

4. Conclusion

In summary, PS/Fe_3O_4 nanocomposites with different particle loadings have been prepared through a solvent extraction method and systematically studied. The NPs were well distributed in the PS matrix with 5, 10, and 20 wt % without obvious agglomeration in the micron dimension with strong interaction between PS and NPs. In addition, the average crystallite size of the Fe_3O_4 NPs with a loading of 10 wt% is about 13.59 nm, and the intensity of these diffraction peaks of the Fe_3O_4 NPs becomes stronger with increasing the NP loadings. Meanwhile, the thermal stability of the PS/Fe_3O_4 PNCs was enhanced and the flammability of PS matrix was suppressed by adding these Fe_3O_4 NPs. Both glass transition temperature (T_g) and melting temperature (T_m) were increased with increasing Fe_3O_4 NPs loadings. The observed monotonically decreased complex viscosity indicated a strong shear thinning behavior in the PNCs; Furthermore, the percolation took place at low frequency range (0.1–1 Hz) when the NPs were introduced in the matrix. The PS/Fe_3O_4 PNCs exhibit superparamagnetic behavior at room temperature. In addition enhanced dielectric properties was related to the Fe_3O_4 NP loadings.

Acknowledgments: This project was supported by the research start-up fund and research enhancement grant from Lamar University. Partial financial supports from NSF—Nanomanufacturing (CMMI-13-14486), Nanoscale Interdisciplinary Research Team and Materials Processing and Manufacturing (CMMI 10-30755), and Chemical and Biological Separations (CBET 11-37441) are acknowledged.

Received: May 18, 2013; Revised: June 20, 2013; Published online: September 3, 2013; DOI: 10.1002/mame.201300208

Keywords: flammability; nanocomposites; permittivity; polystyrene; thermomechanical properties

[1] P. Kim, N. M. Doss, J. P. Tillotson, P. J. Hotchkiss, M. J. Pan, S. R. Marder, J. Li, J. P. Calame, J. W. Perry, *ACS Nano* **2009**, *3*, 2581.

[2] T. Shimada, K. Ookubo, N. Komuro, T. Shimizu, N. Uehara, *Langmuir* **2007**, *23*, 11225.
[3] T. Kashiwagi, F. Du, J. F. Douglas, K. I. Winey, R. H. Harris, J. R. Shields, *Nat. Mater.* **2005**, *4*, 928.
[4] Z. Guo, S.-E. Lee, H. Kim, S. Park, H. Hahn, A. Karki, D. Young, *Acta Mater.* **2009**, *57*, 267.
[5] Z. Guo, S. Park, H. T. Hahn, S. Wei, M. Moldovan, A. B. Karki, D. P. Young, *J. Appl. Phys.* **2007**, *101*, 09M511.
[6] Q. Dai, D. Berman, K. Virwani, J. Frommer, P. O. Jubert, M. Lam, T. Topuria, W. Imaino, A. Nelson, *Nano Lett.* **2010**, *10*, 3216.
[7] J. Zhu, S. Wei, L. Zhang, Y. Mao, J. Ryu, A. B. Karki, D. P. Young, Z. Guo, *J. Mater. Chem.* **2010**, *21*, 342.
[8] O. Breuer, U. Sundararaj, *Polym. Compos.* **2004**, *25*, 630.
[9] J. Zhu, S. Wei, D. Rutman, N. Haldolaarachchige, D. P. Young, Z. Guo, *Polymer* **2011**, *52*, 2947.
[10] X. Chen, S. Wei, C. Gunesoglu, J. Zhu, C. S. Southworth, L. Sun, A. B. Karki, D. P. Young, Z. Guo, *Macromol. Chem. Phys.* **2010**, *211*, 1775.
[11] B. Lin, G. A. Gelves, J. A. Haber, P. Pötschke, U. Sundararaj, *Macromol. Chem. Phys.* **2008**, *293*, 631.
[12] U. Lange, S. Ivanov, V. Lyutov, V. Tsakova, V. M. Mirsky, *J. Solid State Electrochem.* **2010**, *14*, 1261.
[13] J. Zhu, S. Wei, J. Ryu, L. Sun, Z. Luo, Z. Guo, *ACS Appl. Mater. Interfaces* **2010**, *2*, 2100.
[14] S. Khanna, S. Linderoth, *Phys. Rev. Lett.* **1991**, *67*, 742.
[15] X. Lin, C. Sorensen, K. Klabunde, G. Hadjipanayis, *Langmuir* **1998**, *14*, 7140.
[16] S. Apsel, J. Emmert, J. Deng, L. Bloomfield, *Phys. Rev. Lett.* **1996**, *76*, 1441.
[17] J. Zhu, S. Wei, J. Ryu, M. Budhathoki, G. Liang, Z. Guo, *J. Mater. Chem.* **2010**, *20*, 4937.
[18] Z. Guo, T. Y. Kim, K. Lei, T. Pereira, J. G. Sugar, H. T. Hahn, *Compos. Sci. Technol.* **2008**, *68*, 164.
[19] R. F. Ziolo, E. P. Giannelis, B. A. Weinstein, M. P. O'horo, B. N. Ganguly, V. Mehrotra, M. W. Russell, D. R. Huffman, *Science* **1992**, *257*, 219.
[20] J. Zhu, S. Wei, Y. Li, L. Sun, N. Haldolaarachchige, D. P. Young, C. Southworth, A. Khasanov, Z. Luo, Z. Guo, *Macromolecules* **2011**, *44*, 4382.
[21] B. Zapotoczny, M. Dudek, J. Kozio, J. Mleczko, *Phys. A* **2013**, *392*, 1493.
[22] Z. Huang, F. Tang, *J. Colloid Interface Sci.* **2004**, *275*, 142.
[23] J.-L. Zhao, R. Yi, *Polym. Mater. Sci. Eng.* **2009**, *10*, 30.
[24] W. Zhong, P. Liu, H. Shi, D. Xue, *Express Polym. Lett.* **2010**, *4*, 183.
[25] D. Shi, H. S. Cho, Y. Chen, H. Xu, H. Gu, J. Lian, W. Wang, G. Liu, C. Huth, L. Wang, *Adv. Mater.* **2009**, *21*, 2170.
[26] J. Sun, S. Zhou, P. Hou, Y. Yang, J. Weng, X. Li, M. Li, *J. Biomed. Res. A* **2007**, *80*, 333.
[27] J. Zhang, J. Chen, Z. Wang, *Mater. Lett.* **2007**, *61*, 1629.
[28] J. Deng, X. Ding, W. Zhang, Y. Peng, J. Wang, X. Long, P. Li, A. S. C. Chan, *Polymer* **2002**, *43*, 2179.
[29] L. Qiu, W. Chen, B. Qu, *Polym. Degrad. Stab.* **2005**, *87*, 433.
[30] D. Wu, X. Ge, Y. Huang, Z. Zhang, Q. Ye, *Mater. Lett.* **2003**, *57*, 3549.
[31] D. Wu, X. Ge, Z. Zhang, M. Wang, S. Zhang, *Langmuir* **2004**, *20*, 5192.
[32] M. Mahmoudi, A. Simchi, M. Imani, A. S. Milani, P. Stroeve, *Nanotechnology* **2009**, *20*, 225104.
[33] L. M. Liz-Marzan, P. V. Kamat, *Nanoscale Materials*, Springer, New York **2003**.
[34] M. Xiao, L. Sun, J. Liu, Y. Li, K. Gong, *Polymer* **2002**, *43*, 2245.
[35] B. N. Jang, M. Costache, C. A. Wilkie, *Polymer* **2005**, *46*, 10678.
[36] Q. Zhao, E. T. Samulski, *Polymer* **2006**, *47*, 663.
[37] K. Saeed, S. Y. Park, H. J. Lee, J. B. Baek, W. S. Huh, *Polymer* **2006**, *47*, 8019.
[38] A. Chatterjee, B. Deopura, *J. Appl. Polym. Sci.* **2006**, *100*, 3574.
[39] T. Monakhova, P. Nedorezova, T. Bogayevskaya, V. Tsvetkova, Y. A. Shlyapnikov, *Polym. Sci. USSR* **1988**, *30*, 2589.
[40] P. Uthirakumar, K. S. Nahm, Y. B. Hahn, Y. S. Lee, *Eur. Polym. J.* **2004**, *40*, 2437.
[41] K. Wakabayashi, P. J. Brunner, J. Masuda, S. A. Hewlett, J. M. Torkelson, *Polymer* **2010**, *51*, 5525.
[42] V. Babrauskas, R. D. Peacock, *Fire Safety J.* **1992**, *18*, 255.
[43] C. Q. Yang, Q. He, R. E. Lyon, Y. Hu, *Polym. Degrad. Stab.* **2010**, *95*, 108.
[44] D. W. Chae, K. J. Kim, B. C. Kim, *Polymer* **2006**, *47*, 3609.
[45] H. Gu, S. Tadakamalla, Y. Huang, H. A. Colorado, Z. Luo, N. Haldolaarachchige, D. P. Young, S. Wei, Z. Guo, *ACS Appl. Mater. Interfaces* **2012**, *4*, 5613.
[46] H. B. Hsueh, C. Y. Chen, *Polymer* **2003**, *44*, 5275.
[47] T. Liu, I. Y. Phang, L. Shen, S. Y. Chow, W.-D. Zhang, *Macromolecules* **2004**, *37*, 7214.
[48] S. K. Nayak, S. Mohanty, *J. Appl. Polym. Sci.* **2009**, *112*, 778.
[49] J. Zhu, S. Wei, A. Yadav, Z. Guo, *Polymer* **2010**, *51*, 2643.
[50] P. Pötschke, M. Abdel-Goad, I. Alig, S. Dudkin, D. Lellinger, *Polymer* **2004**, *45*, 8863.
[51] C. A. Mitchell, J. L. Bahr, S. Arepalli, M. James, R. Krishnamoorti, *Macromolecules* **2002**, *35*, 8825.
[52] M. Sugimoto, T. Tanaka, Y. Masubuchi, J. I. Takimoto, K. Koyama, *J. Appl. Polym. Sci.* **1999**, *73*, 1493.
[53] Z. Guo, L. L. Henry, V. Palshin, E. J. Podlaha, *J. Mater. Chem.* **2005**, *16*, 1772.
[54] D. Zhang, A. B. Karki, D. Rutman, D. P. Young, A. Wang, D. Cocke, T. H. Ho, Z. Guo, *Polymer* **2009**, *50*, 4189.
[55] S. Xuan, L. Hao, W. Jiang, X. Gong, Y. Hu, Z. Chen, *J. Magn. Magn. Mater.* **2007**, *308*, 210.
[56] P. Hu, S. Zhang, H. Wang, D. Pan, J. Tian, Z. Tang, A. A. Volinsky, *J. Alloys Compd.* **2011**, *509*, 2316.
[57] X. Chen, S. Wei, A. Yadav, R. Patil, J. Zhu, R. Ximenes, L. Sun, Z. Guo, *Macromol. Mater. Eng.* **2011**, *296*, 434.
[58] H. S. Nalwa, *Handbook of Low and High Dielectric Constant Materials and Their Applications, Two-Volume Set*, Academic Press, Burlington **1999**.
[59] P. Barber, S. Balasubramanian, Y. Anguchamy, S. Gong, A. Wibowo, H. Gao, H. J. Ploehn, H. C. Zur Loye, *Materials* **2009**, *2*, 1697.
[60] J. Zhu, S. Wei, J. Ryu, Z. Guo, *J. Phys. Chem. C* **2011**, *115*, 13215.
[61] Z. M. Dang, L. Wang, Y. Yin, Q. Zhang, *Adv. Mater.* **2007**, *19*, 852.
[62] Q. He, T. Yuan, J. Zhu, Z. Luo, N. Haldolaarachchige, L. Sun, A. Khasanov, Y. Li, D. P. Young, S. Wei, *Polymer* **2012**, *53*, 3642.
[63] T. saka, M. Datta, *Energy Storage Systems in Electronics*, Vol. 1, CRC Press, Boca Raton **2000**.